MSDE

Molecular Systems Design & Engineering

rsc.li/molecular-engineering

ISSN 2058-9689

ROYAL SOCIETY OF CHEMISTRY

IChemE

ROYAL SOCIETY OF CHEMISTRY

rsc.li/molecular-engineering

Design, System, Application Statement

We present a constrained inverse design strategy that uses relative-entropy minimization to discover simple, experimentally relevant pair potentials for binary colloidal mixtures. By imposing physically motivated constraints inspired by DNA-functionalized nanoparticles, the design space is reduced to parameters directly linked to experimentally tunable variables, enabling the assembly of complex two- and three-dimensional superlattices, including honeycomb and cubic diamond. The system studied, binary colloidal particles with tunable attractions and repulsions, is broadly important for engineering materials with tailored optical, photonic, and catalytic properties. By focusing on experimentally realizable interaction forms rather than highly flexible spline potentials, we show that even low-coordination lattices can be assembled robustly while maintaining a clear path toward physical implementation. This work bridges the gap between computational inverse design and experimental colloidal self-assembly, providing a practical framework to design and realize functional materials with complex architectures.

Design of simple interactions to assemble complex crystals from binary mixtures of colloidal particles

Beth Hsiao-Yen Wei,[1, a)] C. Levi Petix,[2, a)] Qizan Chen,[1] Michael P. Howard,[2, b)] and Jeetain Mittal[1, 3, 4, c)]

[1)] *Artie McFerrin Department of Chemical Engineering, Texas A&M University, College Station*

[2)] *Department of Chemical Engineering, Auburn University, Auburn, AL 36849, USA*

[3)] *Department of Chemistry, Texas A&M University, College Station*

[4)] *Interdisciplinary Graduate Program in Genetics and Genomics, Texas A&M University, College Station*

Computational methods for designing interactions between colloidal particles that induce self-assembly have received much attention for their promise to discover tailored materials. However, it often remains a challenge to translate computationally designed interactions to experiments because they may have features that are too complex, or even infeasible, to physically realize. Toward bridging this gap, we leverage relative-entropy minimization to design pair potentials for binary mixtures of colloidal particles that assemble crystal superlattices. We reduce the dimensionality and extent of the interaction design space by enforcing constraints on the form and parametrization of the pair potentials that are physically motivated by DNA-functionalized nanoparticles. We show that several two- and three-dimensional lattices, including honeycomb and cubic diamond, can be assembled using simple interactions despite their complex structures. We also find that the initial conditions used for the designed parameters as well as the assembly protocol play important roles in determining the outcome and success of the assembly process.

[a)] These authors contributed equally.

[b)] Electronic mail: mphoward@auburn.edu

[c)] Electronic mail: jeetain@tamu.edu

Molecular Systems Design & Engineering Accepted Manuscript

I. INTRODUCTION

The self-assembly of colloidal particles into crystal superlattices has important applications in the fabrication of optical,[1] catalytic[2] and plasmonic materials.[3] Particle properties such as shape,[4] patchiness,[5,6] size,[7] charge[8,9] and surface functionalization[10] can be engineered to control the structure of the superlattice and its corresponding properties.[11,12] Characterizing the different superlattices that are produced from such a vast design space using traditional "forward" experimentation can be expensive and slow, motivating the use of "inverse" methods that efficiently identify particles that yield desired structures. Inverse-design methods for self-assembly typically consist of a loss function that measures how different the produced structure is from the desired one and an optimization strategy that minimizes the loss function with respect to the particle properties that can be varied.[13] These methods include both approaches physically grounded in statistical mechanics,[14–17] such as free-energy landscape engineering,[18,19] relative-entropy minimization,[20–26] and digital alchemy,[27,28] as well as data-driven strategies that exploit machine learning.[29–32]

While inverse design has had considerable computational success[13,33] in identifying interactions for specific target structures—avoiding exhaustive parameter sweeps[34,35] that identify all structures in a space and become prohibitive in high-dimensional space— translation to experiment remains far more limited.[36–39] One major challenge is that pairwise potential energy functions, representing the effective interaction between two particles, are typically designed computationally, but creating particles that will produce these interactions can be difficult if the pair potentials do not have physically interpretable parameters. Pair potentials having no experimental realization may even be designed if physical requirements are not enforced in the optimization. For example, relative-entropy minimization has been successfully applied many times to design pair potentials represented using Akima splines.[20–23,26,40] Splines have great flexibility in the functions they can represent and so are useful for finding a feasible design, but this flexibility may produce features such as high-frequency oscillations or plateaus that do not readily map to a known particle surface chemistry. Spline potentials can be constrained[20] or filtered[40] to remove some of these features, but the resulting interactions are still typically challenging to realize. Beyond spline representations, functional forms with many adjustable parameters can also yield interactions that are hard to realize experimentally.[41,42] Using multiple types of particles has also been proposed as

a strategy to simplify interaction complexity at the expense of compositional complexity;[43] however, spline potentials designed for binary mixtures of particles using relative-entropy minimization were not necessarily simpler than those designed for equivalent one-component assemblies.[23]

We postulate that this challenge is not caused by a nonexistence of experimentally producible designs. The loss function guiding the design may have local minima and/or regions with low curvature near a global minimum, suggesting that other, simpler interactions may produce acceptable or near-optimal structures. Indeed, forward modeling has shown that colloidal particles interacting through simple, often experimentally-motivated, pair potentials can assemble a variety of structures.[44–46] However, assembly of open lattices with such potentials remains difficult; cubic diamond has remained particularly challenging despite great interest because of its desirable for photonics properties.[47,48] Additionally, these simple interactions may not be selected by inverse methods if they are less optimal than other, more complex interactions that are admissible. Inverse-design methods can be forced to consider only these simpler interactions by designing physically motivated pair potentials with parameters that are directly related to experimentally controllable variables.[49–51] The trade-off is that it may now be more difficult, or even impossible, to produce the desired structure than with a spline potential because the particle interactions are more constrained.

At the same time, DNA-functionalized particles (DFPs) are known to be a versatile material platform of particular interest for colloidal self-assembly. Simple pair potentials,[52–54] including Fermi–Jagla[55,56] and Lennard-Jones-nm[57] potentials, have been developed to capture the effective interactions between DFPs, such as hybridization-driven attraction and repulsion due to chain overlaps, and have been experimentally validated.[58–63] While experimental self-assembly of single-component crystals has mostly been limited to simple close-packed structures,[62,64,65] binary mixtures of DFPs offer a richer design space because stoichiometry and differences in particle interactions can be exploited to stabilize structures that would be inaccessible with only a single type of DFP.[62,66]

In this work, we use relative-entropy minimization to optimize pair potentials for binary mixtures of colloidal particles under physical constraints that reflect known features of DFP interactions, namely tunable repulsion ranges and attraction strengths, as well as symmetries of the superlattice. Our goal is to show that simple interactions can be designed to assemble complex crystal superlattices for binary particle mixtures, even though they should not

form with only one particle type. We target four lattices of varying complexity: square and honeycomb in two dimensions as well as body-centered cubic (BCC) and cubic diamond in three dimensions. We demonstrate that all these superlattices can be successfully designed for using a bulk isochoric temperature cycling protocol; however, we find that only some designs subsequently reliably self-assemble under bulk isothermal compression. We show that one reason for this behavior may be sensitivity to the initial choice of parameters for optimization, consistent with our postulation about the viability of multiple designs. We additionally probe how our designed interactions perform under dilute conditions typically used in experiments, highlighting the important role of protocol in both the design and assembly processes.

II. MODEL AND METHODS

We employed the perturbed Lennard-Jones pair potential[67,68] as a simple model that captures the essential physics of DFP interactions, namely tunable repulsion and attraction; alternative models for DFPs could be used within the same framework if desired. Specifically, the pair potential u_{ij} between two particles of types i and j was

$$u_{ij}(r) = \begin{cases} u_{ij}^{\text{LJ}}(r) + (1 - \lambda_{ij})\varepsilon_{ij}, & r \leq 2^{1/6}\sigma_{ij} \\ \lambda_{ij}u_{ij}^{\text{LJ}}(r), & \text{otherwise} \end{cases}, \tag{1}$$

where u_{ij}^{LJ} is the standard Lennard-Jones potential,

$$u_{ij}^{\text{LJ}}(r) = 4\varepsilon_{ij}\left[\left(\frac{\sigma_{ij}}{r}\right)^{12} - \left(\frac{\sigma_{ij}}{r}\right)^{6}\right], \tag{2}$$

r is the distance between the centers of the particles, ε_{ij} is the interaction energy, σ_{ij} is the interaction length, and λ_{ij} modulates the strength of the attractive tail of u_{ij} independently of its repulsive core. When $\lambda_{ij} = 1$, u_{ij} is the Lennard-Jones potential; when $\lambda_{ij} = 0$, u_{ij} is the purely repulsive Weeks–Chandler–Andersen potential; and when $0 < \lambda_{ij} < 1$, u_{ij} has the same repulsion but less attraction than the Lennard-Jones potential. This pair potential is similar to that used in ref. 57 to map to a tunable interaction in DNA-functionalized nanoparticles; we refer readers interested in the details of how the experimental potentials are tuned to that work.

Our target crystal superlattices (Table S1) are formed from binary mixtures containing particles of types A and B, so in principle, 9 parameters are needed to specify the potential

energy function corresponding to eq. (1). However, we were able to reduce the dimensionality and size of this design space using physical insights, which is an advantage of performing inverse design using a physically motivated pair potential. Specifically, we assumed that all particles had the same repulsion strength, coming primarily from the core nanoparticle and grafted DNA chains, at the design temperature, so $\varepsilon_{\mathrm{AA}} = \varepsilon_{\mathrm{AB}} = \varepsilon_{\mathrm{BB}} = \varepsilon$, where ε can be considered the unit of energy. Further, the symmetry of the 4 lattices we designed (Fig. 1, Table S1) implies that $\sigma_{\mathrm{AA}} = \sigma_{\mathrm{BB}}$ and $\lambda_{\mathrm{AA}} = \lambda_{\mathrm{BB}}$. Hence, only σ_{AA}, σ_{AB}, λ_{AA}, and λ_{AB} needed to be treated as independent parameters. In preliminary tests, we found σ_{ij} to be numerically challenging to optimize concurrently with λ_{ij} because eq. (1) is a highly nonlinear function of σ_{ij}. We accordingly considered 4 parameters $\boldsymbol{\theta} = (\sigma_{\mathrm{AA}}^6, \sigma_{\mathrm{AB}}^6, \lambda_{\mathrm{AA}}, \lambda_{\mathrm{AB}})$ for optimization. Based on forward modeling and experiments,[57,69,70] we constrained this parameter space to be consistent with $0.5\,\sigma \leq \sigma_{ij} \leq 2\,\sigma$ and $0 \leq \lambda_{ij} \leq 1$, where σ is the unit of length.
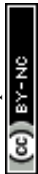
To design the parameters $\boldsymbol{\theta}$ that self-assembled a specific lattice, we minimized the relative entropy,[22,71,72]

$$S_{\mathrm{rel}}(\boldsymbol{\theta}) = \int \mathrm{d}\mathbf{R}\, p_0(\mathbf{R}) \ln\left[\frac{p_0(\mathbf{R})}{p(\mathbf{R};\boldsymbol{\theta})}\right]. \tag{3}$$

Here, $p_0(\mathbf{R})$ is the probability density function to observe a given configuration of particles $\mathbf{R}$ in a target ensemble of structures, while $p(\mathbf{R};\boldsymbol{\theta})$ is the probability density function to observe the same configuration in a model ensemble where particles interact according to eq. (1) with parameters given by $\boldsymbol{\theta}$. The relative entropy is zero when p is identical to p_0 and positive otherwise, so S_{rel} is a loss function that can be minimized with respect to $\boldsymbol{\theta}$ to make the model ensemble resemble the target ensemble. For a multicomponent mixture at thermodynamic equilibrium in the canonical ensemble (constant temperature T, volume V, and number of particles N_i for each type i), the gradient of S_{rel} with respect to $\boldsymbol{\theta}$ is[73,74]

$$\frac{\partial S_{\mathrm{rel}}}{\partial \boldsymbol{\theta}} = \sum_i \sum_j \frac{2\pi\beta N_i N_j}{V}$$
$$\times \int_0^\infty \mathrm{d}r\, r^2 \left[g_0^{(ij)}(r) - g^{(ij)}(r;\boldsymbol{\theta})\right] \frac{\partial u_{ij}}{\partial \boldsymbol{\theta}}, \tag{4}$$

where the sums are taken over all particle types, $\beta = 1/(k_{\mathrm{B}}T)$ with the Boltzmann constant k_{B}, and $g_0^{(ij)}(r)$ and $g^{(ij)}(r;\boldsymbol{\theta})$ are the radial distribution functions for particles of types i and j in the target and model ensembles, respectively. Although eq. (3) cannot be readily evaluated for most systems, eq. (4) can and so can be used to minimize S_{rel} with gradient-

based methods. In practice, $g_0^{(ij)}$ is prescribed by the desired target structure, while $g^{(ij)}$ must be simulated for a given $\boldsymbol{\theta}$.

To evaluate $g_0^{(ij)}$, initial configurations that contained at least 1000 total particles were generated at a number density and stoichiometry consistent with the target structure (Table S1). Each particle was tethered to a lattice site by a harmonic potential $\phi(r) = kr^2/2$, where r is the distance of the center of the particle from the lattice site and k is a spring constant. A target ensemble of particle configurations was then simulated by drawing an independent random displacement for each particle from a Gaussian distribution with zero mean and variance $(\beta k)^{-1}$. We chose a spring constant $k = 1000\,\varepsilon/\sigma^2$, which we found to produce well-defined but numerically integrable peaks in $g_0^{(ij)}$, and used 1000 configurations to compute $g_0^{(ij)}$ up to a distance of $5\,\sigma$ with a bin spacing of $0.05\,\sigma$.

Relative-entropy minimization was carried out with relentless[73] (version 0.1.1 with operations modified to support volume resizing) using HOOMD-blue[75] (version 2.9.7). Langevin dynamics simulations were performed to evaluate $g^{(ij)}$ in eq. (4). The simulation timestep was $0.001\,\tau$ and the particle friction factor was $0.1\,m/\tau$, where m is the mass of a particle (taken to be the same for both types) and $\tau = \sqrt{m\sigma^2/\varepsilon}$ is the unit of time. The particles were initialized in the target structure, then equilibrated for $3 \times 10^4\,\tau$ at temperature $T = 3\,\varepsilon/k_{\mathrm{B}}$ to attempt to melt the crystal. We found this initialization protocol to be necessary because it was often not possible to place the particles in randomized or fluid-like configurations without overlap for suboptimal values of σ_{ij}. The temperature was then slowly quenched from $3\,\varepsilon/k_{\mathrm{B}}$ to $1\,\varepsilon/k_{\mathrm{B}}$ over $2 \times 10^4\,\tau$ at a constant rate. The radial distribution function $g^{(ij)}$ was finally sampled every $10\,\tau$ during a $10^4\,\tau$ production period with the same maximum distance and bin spacing as was used for $g_0^{(ij)}$. The parameters $\boldsymbol{\theta}$ were then adjusted to attempt to minimize S_{rel} using gradient descent with a step size chosen for each parameter such that the change in σ_{ij}^6 was approximately $0.25\,\sigma^6$ and the change in λ_{ij} was approximately 0.05 for the first iteration. We initialized σ_{ij}^6 to be consistent with the position of the first peak in $g_0^{(ij)}$ based on physical knowledge that it relates to the size of the particle and DNA corona, while λ_{AA} and λ_{AB} were initialized to 0 and 1, respectively, based on previous work.[43,57] The optimization was considered converged when the absolute values of all components of the gradient were less than 0.01 in their respective units or further progress could not be made due to the box constraints on the parameters.

III.   RESULTS AND DISCUSSION

A.   Initial design

We carried out our inverse-design procedure starting with the square lattice in two-dimensions (Fig. 1a–c). The procedure quickly converged, finding an interaction between like particles that was purely repulsive and an interaction between unlike particles that was attractive; λ_{AA} and λ_{AB} remained at their initial values of 0 and 1, respectively, throughout the optimization (Fig. S1). We found that σ_{AA} also remained close to its initial value at the first peak in $g_0^{(AA)}$, but σ_{AB} somewhat decreased from its initial value at the first peak in $g_0^{(AB)}$. The range of the like-particle repulsions was longer than that of the unlike-particle attractions, which is characteristic of binary DFPs.[69,76] Purely repulsive Akima-spline potentials have been designed to self-assemble the square lattice using both one and two types of particles.[22,23] Those potentials both have complex features, such as shoulders and plateaus, that our constrained design does not.

Encouraged by this success, we proceeded to design the remaining lattices that we anticipated to be more challenging than square: honeycomb (Fig. 1d–f) is a low-coordinated two-dimensional lattice, BCC (Fig. 1g–i) is a three-dimensional lattice, and cubic diamond (Fig. 1j–l) is a low-coordinated three-dimensional lattice. As for the square lattice, σ_{AA} typically remained close to its initial value, set by the first peak in $g_0^{(AA)}$, but σ_{AB} tended to decrease for all three structures (Fig. S1). For honeycomb, λ_{AB} departed from its initial value but quickly returned; the same happened with λ_{AA} for BCC. Hence, the interactions for both honeycomb and BCC were purely repulsive between like particles and a Lennard-Jones attraction between unlike particles. Interestingly, the cubic diamond was found to have a nonzero λ_{AA} when the optimization converged, corresponding to a weak attraction between like particles in addition to a Lennard-Jones attraction between unlike particles. Such attraction can be achieved by mixing two different DNA strands on each particle[78,79] or via linker-mediated binding.[79]

Overall, our designed interactions are consistent with a pattern observed in a forward modeling study of DFPs:[57] the denser crystals (square and BCC) were assembled by competing repulsive and attractive interactions that were closer in range than those of the less dense crystals (honeycomb and cubic diamond). For the less dense crystals, such long-ranged
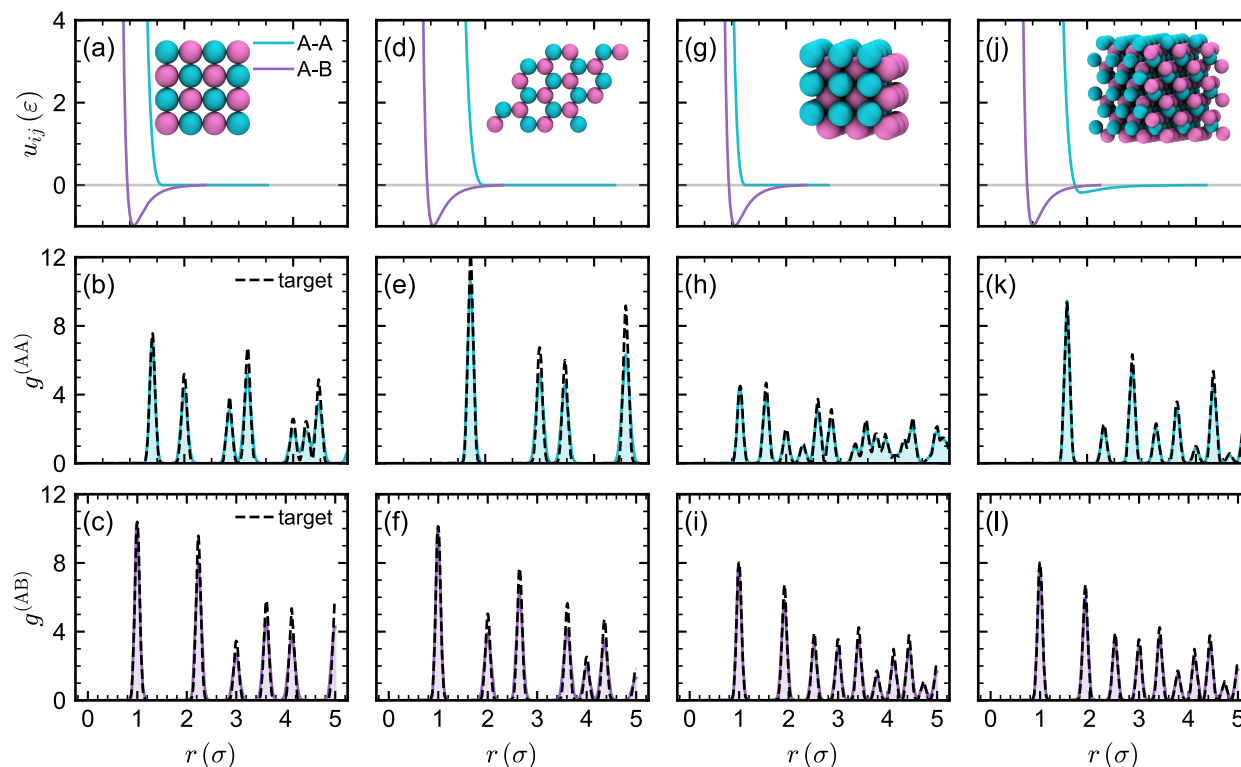
FIG. 1. Designed pair potentials and representative snapshots for each crystal (top row) along with $g^{(ij)}$ measured between like (middle row, filled line) and unlike (bottom row, filled line) particles, compared to the target $g_0^{(ij)}$ (dashed line). The four crystal structures are: (a)–(c) square, (d)–(f) honeycomb, (g)–(i) BCC, and (j)–(l) cubic diamond. Snapshots of the target structures (inset) were rendered using VMD (version 1.9.4).[77]

repulsions between like particles can be attained in experiments by shifting the location of the complementary "sticky" DNA sequence from the tail to the middle of the molecule to enhance shell overlap.[57] The difference in ranges can be approximately quantified through σ_{AB}/σ_{AA}, which was about 1.5 (square) and 1.2 (BCC) for the more dense crystal structures and about 1.9 for the less dense crystals (Table S2). This finding is analogous to previous studies that demonstrated the influence of interaction ranges on DFP self-assembly, for instance, different DNA-linker to particle size ratios producing different structures.[62,80,81]

We further note that it appeared that some of the interaction parameters would slowly evolve with more iterations of gradient descent, particularly for challenging designs like cubic diamond (Fig. S7); however, the optimization stopped because the convergence criteria were satisfied. To investigate whether continued optimization would improve the design, we

performed additional iterations with an order of magnitude stricter tolerance. As expected, the parameters continued to evolve but eventually converge (Fig. S2). Counterintuitively, these converged variables performed worse during isothermal compression, producing more polymorphic crystals with greater variability between independent simulations compared to the original convergence criterion (Fig. S3). This behavior reflects our operational definition of convergence, under which the parameters are considered converged even though small changes may continue with further iterations. The target $g^{(ij)}$ were also well-matched at both convergence thresholds, supporting the notion that multiple acceptable designs exist within a relatively shallow region of the relative entropy function landscape and that some designs may be more robust under different assembly protocols depending on the specific numerical details of the optimization procedure. The design that is found depends on the optimization method, convergence criteria, and initial guess. We will discuss some of these considerations later.

B. Validation of design

Inverse design using the relative entropy is sensitive to the simulation protocol because eq. (4) assumes thermodynamic equilibrium, but equilibrium may not be achieved in a self-assembly simulation for a variety of reasons. For example, a crystal may not nucleate and grow if the simulation time is too short, or there may be crystal defects that cannot anneal. For our simulation protocol, we found that none of the initially crystalline particle configurations were actually able to melt during isochoric temperature cycling despite heating to $T = 3\,\varepsilon/k_{\mathrm{B}}$. Lack of melting may indicate thermodynamic stability of the crystal due to a good initial guess of parameters, but it is also possible the crystal is only metastable or the particles are kinetically trapped. Alternative protocols such as designing under isobaric conditions could help circumvent these issues, but can be numerically challenging.[82]

We hence simulated another assembly protocol based on isothermal compression to validate the interactions we designed using isochoric temperature cycling. We placed the same number of particles quasi-randomly in a simulation box whose edge lengths were three times longer than that of the target, then compressed the box isothermally at $T = 1\,\varepsilon/k_{\mathrm{B}}$ to its target size by reducing the edge lengths at a constant rate over a period of $5 \times 10^4\,\tau$. The particles in the expanded box were gas-like, so they were required to assemble in the vali-
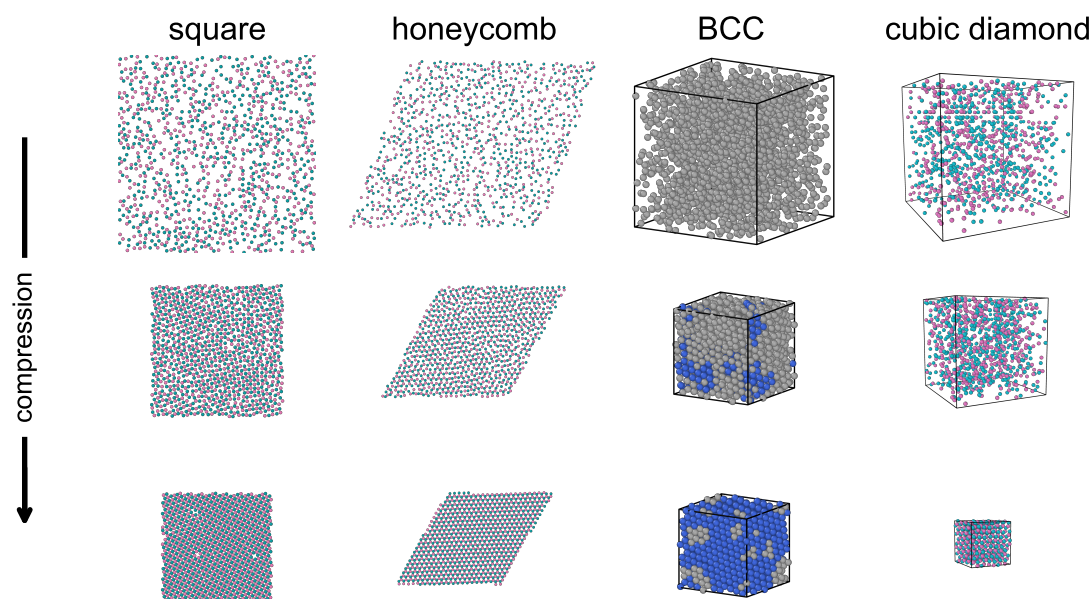
FIG. 2. Snapshots from the first validation (isothermal compression) simulation using the potential designed during isochoric temperature cycling for square, honeycomb, BCC and, cubic diamond.

dation simulations even if the crystal did not melt in the design simulations (Fig. 2). We then simulated a production period of $10^4\,\tau$, sampling particle configurations every $10^2\,\tau$ for structural analysis. We repeated this procedure 5 times starting from different initial configurations to probe variability.

We are using binary mixtures to assemble the targeted superlattices because the simple interactions we considered are not expected to form them with one particle type; however, from a practical perspective, we may not require perfect compositional order in the final assembled structure. For example, two types of DFPs may have the same nanoparticle core and differ only in their DNA functionalization, making them essentially interchangable in the lattice for properties that depend only on the arrangement of cores. Hence, we employed two different structural metrics that were agnostic to composition to assess if the designed interactions assembled the target structure. The first was based on the radial distribution function g ignoring particle type, which we calculated from the recorded particle configurations up to distance $R = 5\,\sigma$ using bin width $0.05\,\sigma$. We then evaluated the mean squared error (MSE) in g relative to the type-agnostic radial distribution function g_0 for the

target,

$$g\,\mathrm{MSE} = \frac{3}{R^3} \int_0^R \mathrm{d}r\, r^2 \left[g(r) - g_0(r)\right]^2. \tag{5}$$

The MSE in g can be nonzero if the particles are correctly arranged in the lattice but have even small differences in their lattice spacing or fluctuations. Accordingly, we chose to use particle-level structural classifiers as a second, complementary metric. We used common neighbor analysis (cutoff radius $1.6\,\sigma$) to classify particles as being in the square lattice,[55,83] polyhedral template matching to classify particles as being in the honeycomb—equivalent to graphene—and BCC lattices (root mean square deviation cutoff 0.1),[84] and an extended common neighbor analysis that identifies second nearest neighbors of a central atom to classify particles as being in the cubic-diamond lattice.[85] We then calculated the average fraction of particles that were classified as matching the target structure across all sampled configurations. The analysis was performed using OVITO (version 3.12.0) extended for the square lattice.[56]

We found that square, honeycomb, and BCC all reliably self-assembled in our validation simulations, with at least 80% of particles being classified as belonging to the target lattice on average (Fig. 3). The MSE in g was consistently larger in the validation simulations than in the design simulations. There was also significant variability in g MSE, but not as much in the fraction of particles classified as being in the correct lattice (Fig. S5). In contrast, there was essentially no variability in either quantity between 3 independent simulations performed using the design protocol, with essentially all particles being classified as the target structure. To better understand the assemblies formed using the validation protocol, we inspected the type-agnostic g for the different crystals (Fig. S4). We found that although their peaks were typically correctly located, they often had different heights and widths, particularly at longer distances. This behavior is consistent with the presence of defects disrupting long-ranged ordering, which were also visually apparent in particle configurations colored by the structural classifier (Fig. 2).

Cubic diamond, on the other hand, had a large increase in g MSE and decrease in fraction of particles classified (only about 27%) in the validation simulations. There was also significant variability between the 5 independent simulations. The radial distribution functions all showed a lack of long-ranged order, but some also had a few additional small peaks at shorter separation distances that were not present in the target (Fig. S4d). The structural classification method we used for cubic diamond identified a significant fraction of parti-
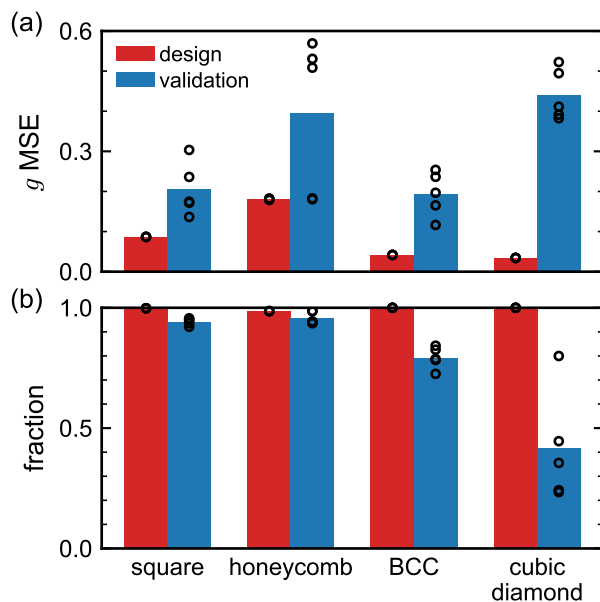
FIG. 3. Average (a) mean squared error (MSE) in type-agnostic radial distribution function g and (b) fraction of particles classified as being in target lattice for design (isochoric temperature cycling, red) and validation (isothermal compression, blue) simulation protocols. To probe variability, we performed 3 independent simulations following the design protocol and 5 independent simulations following the validation protocol; the results from each simulation are shown as open circles.

cles as being hexagonal diamond, a competing polymorph, in some simulations (Fig. S6). Despite their substantial structural differences—75% of rings are boat-like in hexagonal diamond rather than chair-like in cubic diamond—cubic and hexagonal diamond have similar free energies[86,87] and subtly different radial distribution functions, making it difficult to select for only one. Overall, our results indicate substantial polymorphism in the diamond structures produced under bulk isothermal compression that was absent under isochoric temperature cycling, likely due to lack of melting. We confirmed that this polymorphism tended to set in early during compression (Fig. 4a) and persist.

We were curious whether less polymorphism and/or more consistent crystallization might be achievable for cubic diamond by assembling under conditions that more easily allowed for particle rearrangement. In experiments, self-assembly often occurs from a dilute suspension through a gas–solid-like phase transition.[88] Drawing inspiration from this procedure, we initialized simulations in the large simulation box used to start the bulk isothermal compression; however, we now isochorically cooled from $T = 1\,\varepsilon/k_B$ to $0.01\,\varepsilon/k_B$ at a constant rate
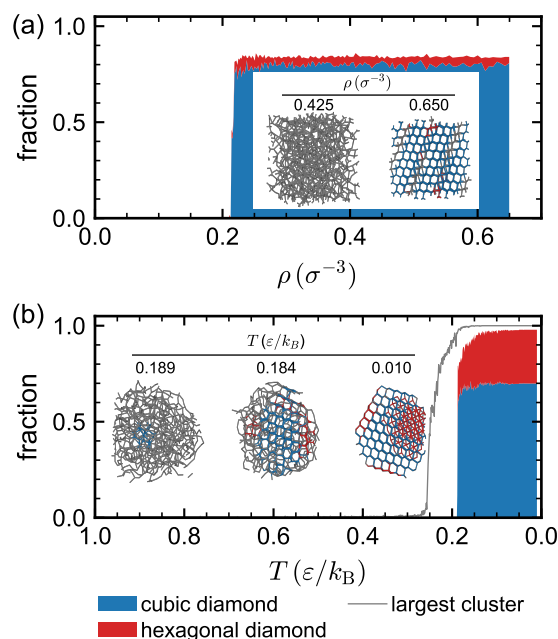
FIG. 4. Representative particle snapshots and fractions of particles classified as cubic or hexagonal diamond as a function of (a) number density ρ during bulk isothermal compression and (b) temperature T during isochoric cooling of an initially dilute suspension. In (b), the grey line is the largest cluster size, indicating that essentially all particles have incorporated into the final crystallite. The particle snapshots show the transition from an amorphous cluster to a crystallite with diamond structure. Snapshots here, in Fig. 5, and in the supplementary information were rendered using OVITO (version 3.12.0).[83]

over a period of $10^5\,\tau$. This slow cooling should drive the particles to self-assemble finite-size crystallites. Indeed, we found that a single crystallite formed at around $T = 0.18\,\varepsilon/k_\mathrm{B}$ by a previously identified two-step mechanism,[57] in which the particles first aggregated into an amorphous cluster then crystallized (Fig. 4b). Like the bulk compression simulations, the final crystallite contained both cubic and hexagonal diamond structures; however, unlike the bulk compression simulations (Fig. S6), there was significantly less variability in the fraction of each structure between independent simulations (Fig. S12). The similar free energies of cubic and hexagonal diamond make it challenging to thermodynamically favor one over the other.[57] We suspect that our isothermal compression protocol inhibited particles' ability to rearrange after nucleation as they continued to densify, leading to more variability than under dilute assembly conditions.

C. Alternative designs

To investigate whether acceptable alternatives to the interactions designed in Section III A may exist, we repeated our inverse-design procedure for the honeycomb lattice with different initial guesses for λ_{AA} and λ_{AB}. We started each of these parameters from either 0 or 1, and we considered all four possible resulting combinations (Fig. S7). We found that the designed interaction between unlike particles was insensitive to the initial value of either λ_{AA} or λ_{AB} and was always attractive, but the designed interaction between like particles was dictated by the initial value of λ_{AA}. Specifically, the designed interaction between like particles was repulsive if $\lambda_{AA} = 0$ initially and attractive if $\lambda_{AA} = 1$ initially. During the design process, λ_{AB} stabilized quickly but λ_{AA} evolved slowly (Fig. S7b,d), suggesting the possibility of convergence of λ_{AA} across a broad range of values depending on the criteria specified. We will compare the two designs that both initially had $\lambda_{AB} = 1$ and either $\lambda_{AA} = 0$ (repulsive like interactions, designated $-+$) or $\lambda_{AA} = 1$ (attractive like interactions, designated $++$).

The $-+$ design produced crystals of similar quality as the $++$ design under bulk isothermal compression (Fig. 5a–b). The $-+$ design had a slightly larger deviation from the target g, but there was less variability between independent simulations (Fig. 5a, Fig. S8). Both designs had nearly all particles classified as being in the target structure (Fig. 5b). However, there were significant differences in assembly from a dilute suspension (Fig. S9). The $-+$ design required significantly colder temperature to assemble than the $++$ design (Fig. 5c–d). Assembly occurred in two steps for the $-+$ design, with string-like structures forming before honeycomb, whereas honeycomb directly nucleated for the $++$ design. The assembled structures for the $-+$ design also tended to be less compact than for the $++$ design (Fig. S9). The structural classifier identified more particles as being honeycomb for the $++$ design than for the $-+$ design; however, this may be partially due to the larger number of interfacial particles in the $-+$ assembly that are more challenging to classify.

The string-like structures for the $-+$ design may be a kinetic effect because the particle dynamics slow considerably as T decreases and assemblies form. To probe this possibility, we ran an additional dilute isochoric simulation where the particles were initialized in the crystallite assembled by the $++$ design, and the temperature was held constant at $T = 0.0755\,\varepsilon/k_B$. This temperature is near the nominal melting point for the $-+$ design estimated from a trace of the potential energy during cooling. We ran a long simulation (duration
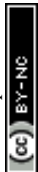
$10^5 \tau$), but the honeycomb crystallite remained stable and strings did not form. We then ran similar simulations at $0.1 \leq k_\mathrm{B}T/\varepsilon \leq 0.5$ at increments of 0.1 (Fig. S13). We found for the $-+$ potential that strings started to detach from the crystallite surface at $T = 0.1\,\varepsilon/k_\mathrm{B}$, and the crystal completely melted at higher temperatures. We performed the same test using the $++$ potential and found that it stabilized the crystallite up to at least $T = 0.3\,\varepsilon/k_\mathrm{B}$. At $T = 0.4\,\varepsilon/k_\mathrm{B}$, there was a coexistence between the crystal and a dilute phase, before complete melting at $T = 0.5\,\varepsilon/k_\mathrm{B}$. This behavior is consistent with the crystallization curves observed in cooling simulations (Fig. 5d).

It has been shown that pair potentials designed for two-dimensional structures can also stabilize their three-dimensional analogs, e.g., a potential designed to self-assemble a square lattice in two dimensions may also self-assemble a simple cubic lattice in three dimensions.[89] We accordingly tested the ability of both our $-+$ and $++$ designs for honeycomb, performed in two dimensions, to form diamond from a dilute suspension in three dimensions. Consistent with our results in two dimensions, we found that the two designs formed distinct structures in three dimensions. In particular, a multilayered graphene-like structure that was not stacked in the manner of graphite was assembled by the $-+$ design (Fig. S10), while the $++$ design assembled mostly cubic and hexagonal diamond as well as their closest neighbors (Fig. S11). Interestingly for the $-+$ design, the particles first formed strings, as in two dimensions (Fig. 5c), before the final structure. We suspect that this structure may also be a kinetic effect for similar reasons as in two dimensions. Overall, the difference in transferability to three dimensions demonstrates another practical difference between the two designs, even though both considered were converged and behaved similarly in bulk simulations.

IV. CONCLUSIONS

We have applied relative-entropy minimization to design isotropic pair potentials for binary mixtures of colloidal particles that self-assemble square and honeycomb superlattices in two dimensions as well as BCC and cubic diamond superlattices in three dimensions. By imposing a functional form on the pair potential that is physically motivated by interactions between DFPs, we restrict the design space in a way that forces simpler interactions to be designed and may enhance experimental realizability. Our results show that these simple
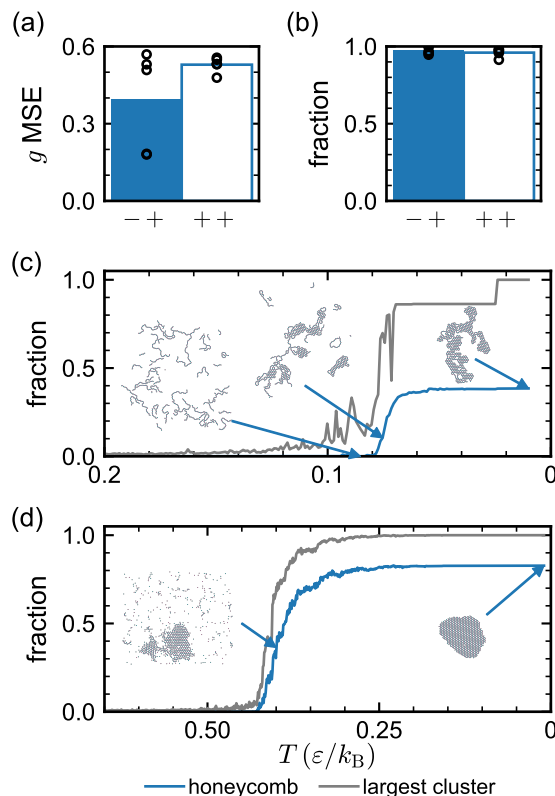
FIG. 5. Average (a) mean squared error (MSE) in type-agnostic radial distribution function g and (b) fraction of particles classified as being in target lattice for 5 independent simulations following validation (isothermal compression) protocol using potentials obtained from inverse-design procedure for honeycomb target starting from $(\lambda_{AA}, \lambda_{AB}) = (0, 1)$, denoted $-+$, or $(1, 1)$, denoted $++$. (c, d) Average fraction of particles classified as honeycomb and fraction of particles in largest cluster as a function of temperature T during isochoric cooling of an initially dilute suspension for $-+$ and $++$ designs. Representative snapshots highlighting differences in the assembly process are also shown.

potentials can still drive assembly of complex lattices, e.g., with low coordination. The approach presented is general and extends naturally to additional target structures with different particle size ratios and stoichiometries beyond those demonstrated here.

A key observation from this work is that multiple viable designs may be identified, depending on the initial parameter guess, but these designs may have rather different behavior under other assembly conditions. We demonstrated this sensitivity by testing several initial values of λ_{ij} in the two-dimensional honeycomb lattice, which showed distinct assem-

bly behavior during validation despite similar performance in the design protocol. While the present study focuses on stoichiometrically balanced binary mixtures, exploring additional compositional complexity may offer additional routes to stabilize or tune targeted structures.[90] Nevertheless, especially complex lattices may require additional design elements beyond composition and isotropic interactions; directional (e.g., patchy) interactions represent one promising approach that can be systematically parameterized and connected to experiments.[91–93] To enhance robustness and practical translation, it may then be important to consider the assembly protocol that will be used in experiments when configuring the computational design protocol. For example, dilute simulations of finite-size crystallites might be used for design rather than simulations of bulk crystals. Moreover, while our design strategy assumes equilibrium thermodynamics, designing for nonequilibrium assembly or processing conditions may also be fruitful.[94,95]

AUTHOR CONTRIBUTIONS

BHW and CLP contributed equally to protocol development, data analysis, visualization, and writing the initial draft of the manuscript. QC assisted with data analysis and visualization. BHW conducted simulations. CLP and MPH developed the software used. MPH and JM conceptualized the project, supervised the work, and provided critical feedback throughout. All authors contributed to discussions and editing of the final manuscript.

CONFLICTS OF INTEREST

There are no conflicts to declare.

DATA AVAILABILITY

The software used to perform the inverse design can be found at https://github.com/mphowardlab/relentless. The parameters of the designed potentials are available as supplementary information. The other data that supports the findings of this study are available from the authors upon reasonable request.

Molecular Systems Design & Engineering Accepted Manuscript

ACKNOWLEDGMENTS

REFERENCES

[1] M. A. Boles, M. Engel, and D. V. Talapin, "Self-assembly of colloidal nanocrystals: From intricate structures to functional materials," Chemical Reviews **116**, 11220–11289 (2016).

[2] Y. Kang, X. Ye, J. Chen, Y. Cai, R. E. Diaz, R. R. Adzic, E. A. Stach, and C. B. Murray, "Design of pt–pd binary superlattices exploiting shape effects and synergistic effects for oxygen reduction reactions," Journal of the American Chemical Society **135**, 42–45 (2013).

[3] D. J. Park, C. Zhang, J. C. Ku, Y. Zhou, G. C. Schatz, and C. A. Mirkin, "Plasmonic photonic crystals realized through dna-programmable assembly," Proceedings of the National Academy of Sciences **112**, 977–981 (2015).

[4] S. Lee and S. C. Glotzer, "Entropically engineered formation of fivefold and icosahedral twinned clusters of colloidal shapes," Nature Communications **13**, 7362 (2022).

[5] S. C. Glotzer and M. J. Solomon, "Anisotropy of building blocks and their assembly into complex structures," Nature Materials **6**, 557–562 (2007).

[6] W. Li, H. Palis, R. Mérindol, J. Majimel, S. Ravaine, and E. Duguet, "Colloidal molecules and patchy particles: complementary concepts, synthesis and self-assembly," Chemical Society Reviews **49**, 1955–1976 (2020).

[7] T. I. Li, R. Sknepnek, R. J. Macfarlane, C. A. Mirkin, and M. Olvera de la Cruz, "Modeling the crystallization of spherical nucleic acid nanoparticle conjugates with molecular dynamics simulations," Nano Letters **12**, 2509–2514 (2012).

[8] A.-P. Hynninen, M. E. Leunissen, A. van Blaaderen, and M. Dijkstra, "Cuau structure in the restricted primitive model and oppositely charged colloids," Physical Review Letters **96**, 018303 (2006).

[9] M. E. Leunissen, C. G. Christova, A.-P. Hynninen, C. P. Royall, A. I. Campbell, A. Imhof, M. Dijkstra, R. van Roij, and A. van Blaaderen, "Ionic colloidal crystals of oppositely charged particles," Nature **437**, 235–240 (2005).

[10] A. Dong, X. Ye, J. Chen, Y. Kang, T. Gordon, J. M. Kikkawa, and C. B. Murray, "A generalized ligand-exchange strategy enabling sequential surface functionalization of colloidal nanocrystals," Journal of the American Chemical Society **133**, 998–1006 (2011).

[11] S. Wang, S. S. Park, C. T. Buru, H. Lin, P.-C. Chen, E. W. Roth, O. K. Farha, and C. A. Mirkin, "Colloidal crystal engineering with metal–organic framework nanoparticles and dna," Nature Communications **11**, 2495 (2020).

[12] G. Posnjak, X. Yin, P. Butler, O. Bienek, M. Dass, S. Lee, I. D. Sharp, and T. Liedl, "Diamond-lattice photonic crystals assembled from dna origami," Science **384**, 781–785 (2024).

[13] Z. M. Sherman, M. P. Howard, B. A. Lindquist, R. B. Jadrich, and T. M. Truskett, "Inverse methods for design of soft materials," The Journal of Chemical Physics **152**, 140902 (2020).

[14] M. C. Rechtsman, F. H. Stillinger, and S. Torquato, "Optimized interactions for targeted self-assembly: Application to a honeycomb lattice," Physical Review Letters **95**, 228301 (2005).

[15] E. Marcotte, F. H. Stillinger, and S. Torquato, "Optimized monotonic convex pair potentials stabilize low-coordinated crystals," Soft Matter **7**, 2332–2335 (2011).

[16] M. C. Rechtsman, F. H. Stillinger, and S. Torquato, "Synthetic diamond and wurtzite structures self-assemble with isotropic pair interactions," Physical Review E **75**, 031403 (2007).

[17] E. Marcotte, F. H. Stillinger, and S. Torquato, "Communication: Designed diamond ground state via optimized isotropic monotonic pair potentials," The Journal of Chemical Physics **138**, 061101 (2013).

[18] A. W. Long and A. L. Ferguson, "Rational design of patchy colloids via landscape engineering," Molecular Systems Design & Engineering **3**, 49–65 (2018).

[19] Y. Ma and A. L. Ferguson, "Inverse design of self-assembling colloidal crystals with omnidirectional photonic bandgaps," Soft Matter **15**, 8808–8826 (2019).

[20] B. A. Lindquist, R. B. Jadrich, W. D. Piñeros, and T. M. Truskett, "Inverse design of self-assembling frank-kasper phases and insights into emergent quasicrystals," The Journal of Physical Chemistry B **122**, 5547–5556 (2018).

[21] R. B. Jadrich, B. A. Lindquist, and T. M. Truskett, "Probabilistic inverse design for self-assembling materials," The Journal of Chemical Physics **146**, 184103 (2017).

[22] B. A. Lindquist, R. B. Jadrich, and T. M. Truskett, "Communication: Inverse design for self-assembly via on-the-fly optimization," The Journal of Chemical Physics **145**, 111101 (2016).

[23] W. D. Piñeros, B. A. Lindquist, R. B. Jadrich, and T. M. Truskett, "Inverse design of multicomponent assemblies," The Journal of Chemical Physics **148**, 104509 (2018).

[24] R. B. Jadrich, J. A. Bollinger, B. A. Lindquist, and T. M. Truskett, "Equilibrium cluster fluids: pair interactions via inverse design," Soft Matter **11**, 9342–9354 (2015).

[25] B. A. Lindquist, S. Dutta, R. B. Jadrich, D. J. Milliron, and T. M. Truskett, "Interactions and design rules for assembly of porous colloidal mesophases," Soft Matter **13**, 1335–1343 (2017).

[26] D. Banerjee, B. A. Lindquist, R. B. Jadrich, and T. M. Truskett, "Assembly of particle strings via isotropic potentials," The Journal of Chemical Physics **150**, 124903 (2019).

[27] G. van Anders, D. Klotsa, A. S. Karas, P. M. Dodd, and S. C. Glotzer, "Digital alchemy for materials design: Colloids and beyond," ACS Nano **9**, 9542–9553 (2015).

[28] L. Y. Rivera-Rivera, T. C. Moore, and S. C. Glotzer, "Inverse design of triblock janus spheres for self-assembly of complex structures in the crystallization slot via digital alchemy," Soft Matter **19**, 2726–2736 (2023).

[29] B. Kim, S. Lee, and J. Kim, "Inverse design of porous materials using artificial neural networks," Science Advances **6**, eaax9324 (2020).

[30] G. M. Coli, E. Boattini, L. Filion, and M. Dijkstra, "Inverse design of soft materials via a deep learning–based evolutionary strategy," Science Advances **8**, eabj6731 (2022).

[31] R. Kumar, G. M. Coli, M. Dijkstra, and S. Sastry, "Inverse design of charged colloidal particle interactions for self assembly into specified crystal structures," The Journal of Chemical Physics **151**, 084109 (2019).

[32] C. Wang, A. Pérez de Alba Ortíz, and M. Dijkstra, "Inverse design method with enhanced sampling for complex open crystals: Application to novel zeolite self-assembly," ACS Nano **19**, 17423–17437 (2025).

Molecular Systems Design & Engineering Accepted Manuscript

[33] M. Dijkstra and E. Luijten, "From predictive modelling to machine learning and reverse engineering of colloidal self-assembly," Nature Materials **20**, 762–773 (2021).

[34] J. Dshemuchadse, P. F. Damasceno, C. L. Phillips, M. Engel, and S. C. Glotzer, "Moving beyond the constraints of chemistry via crystal structure discovery with isotropic multi-well pair potentials," Proceedings of the National Academy of Sciences **118**, e2024034118 (2021).

[35] R. A. LaCour, C. S. Adorf, J. Dshemuchadse, and S. C. Glotzer, "Influence of softness on the stability of binary colloidal crystals," ACS Nano **13**, 13829–13842 (2019).

[36] B. Srinivasan, T. Vo, Y. Zhang, O. Gang, S. Kumar, and V. Venkatasubramanian, "Designing dna-grafted particles that self-assemble into desired crystalline structures using the genetic algorithm," Proceedings of the National Academy of Sciences **110**, 18431–18435 (2013).

[37] H. Liu, M. Matthies, J. Russo, L. Rovigatti, R. P. Narayanan, T. Diep, D. McKeen, O. Gang, N. Stephanopoulos, F. Sciortino, H. Yan, and P. Romano, Flavioand Šulc, "Inverse design of a pyrochlore lattice of dna origami through model-driven experiments," Science **384**, 776–781 (2024).

[38] Y. Geng, G. van Anders, P. M. Dodd, J. Dshemuchadse, and S. C. Glotzer, "Engineering entropy for the inverse design of colloidal crystals from hard shapes," Science Advances **5**, eaaw0514 (2019).

[39] C. X. Du, G. van Anders, J. Dshemuchadse, P. M. Dodd, and S. C. Glotzer, "Inverse design of compression-induced solid – solid transitions in colloids," Molecular Simulation **46**, 1037–1044 (2020).

[40] C. S. Adorf, J. Antonaglia, J. Dshemuchadse, and S. C. Glotzer, "Inverse design of simple pair potentials for the self-assembly of complex structures," The Journal of Chemical Physics **149**, 204102 (2018).

[41] H. Pan and J. Dshemuchadse, "Targeted discovery of low-coordinated crystal structures via tunable particle interactions," ACS Nano **17**, 7157–7169 (2023).

[42] P. Zhou and S. C. Glotzer, "Inverse design of isotropic pair potentials using digital alchemy with a generalized fourier potential," The European Physical Journal B **94**, 243 (2021).

[43] N. A. Mahynski, E. Pretti, V. K. Shen, and J. Mittal, "Using symmetry to elucidate the importance of stoichiometry in colloidal crystal assembly," Nature Communications **10**, 2028 (2019).

[44] A. Kumar and V. Molinero, "Self-assembly of mesophases from nanoparticles," The Journal of Physical Chemistry Letters **8**, 5053–5058 (2017).

[45] E. C. Oğuz, A. Mijailović, and M. Schmiedeberg, "Self-assembly of complex structures in colloid-polymer mixtures," Physical Review E **98**, 052601 (2018).

[46] A. Travesset, "Binary nanoparticle superlattices of soft-particle systems," Proceedings of the National Academy of Sciences **112**, 9563–9567 (2015).

[47] E. Yablonovitch, "Photonic band-gap structures," Journal of the Optical Society of America B: Optical Physics **10**, 283–295 (1993).

[48] A. Moroz, "Three-dimensional complete photonic-band-gap structures in the visible," Physical Review Letters **83**, 5274–5277 (1999).

[49] E. A. Bedolla-Montiel, J. T. Lange, A. Pérez de Alba Ortíz, and M. Dijkstra, "Inverse design of crystals and quasicrystals in a non-additive binary mixture of hard disks," The The Journal of Chemical Physics **160**, 244902 (2024).

[50] B. A. Lindquist, "Inverse design of equilibrium cluster fluids applied to a physically informed model," The Journal of Chemical Physics **154**, 174907 (2021).

[51] N. A. Mahynski, R. Mao, E. Pretti, V. K. Shen, and J. Mittal, "Grand canonical inverse design of multicomponent colloidal crystals," Soft Matter **16**, 3187–3194 (2020).

[52] B. D. Rabideau and R. T. Bonnecaze, "A computational study of the hydrodynamically assisted organization of dna-functionalized colloids in 2d," Langmuir **23**, 10000–10007 (2007).

[53] E. Auyeung, T. I. N. G. Li, A. J. Senesi, A. L. Schmucker, B. C. Pals, M. O. de la Cruz, and C. A. Mirkin, "Dna-mediated nanoparticle crystallization into wulff polyhedra," Nature **505**, 73–77 (2014).

[54] A. V. Tkachenko, "Morphological diversity of dna-colloidal self-assembly," Physical Review Letters **89**, 148303 (2002).

[55] M. Song, Y. Ding, H. Zerze, M. A. Snyder, and J. Mittal, "Binary superlattice design by controlling dna-mediated interactions," Langmuir **34**, 991–998 (2018).

[56] E. Pretti, H. Zerze, M. Song, Y. Ding, N. A. Mahynski, H. W. Hatch, V. K. Shen, and J. Mittal, "Assembly of three-dimensional binary superlattices from multi-flavored particles," Soft Matter **14**, 6303–6312 (2018).

[57] R. Mao, B. Minevich, D. McKeen, Q. Chen, F. Lu, O. Gang, and J. Mittal, "Regulating phase behavior of nanoparticle assemblies through engineering of dna-mediated isotropic

interactions," Proceedings of the National Academy of Sciences **120**, e2302037120 (2023).

[58] M. M. Maye, D. Nykypanchuk, D. van der Lelie, and O. Gang, "Dna-regulated micro- and nanoparticle assembly," Small **3**, 1678–1682 (2007).

[59] W. B. Rogers and V. N. Manoharan, "Programming colloidal phase transitions with dna strand displacement," Science **347**, 639–642 (2015).

[60] C. A. Mirkin, R. L. Letsinger, R. C. Mucic, and J. J. Storhoff, "A dna-based method for rationally assembling nanoparticles into macroscopic materials," Nature **382**, 607–609 (1996).

[61] E. W. Gehrels, W. B. Rogers, and V. N. Manoharan, "Using dna strand displacement to control interactions in dna-grafted colloids," Soft Matter **14**, 969–984 (2018).

[62] R. J. Macfarlane, B. Lee, M. R. Jones, N. Harris, G. C. Schatz, and C. A. Mirkin, "Nanoparticle superlattice engineering with dna," Science **334**, 204–208 (2011).

[63] M. Dwivedi, S. L. Singh, A. S. Bharadwaj, V. Kishore, and A. V. Singh, "Self-assembly of dna-grafted colloids: A review of challenges," Micromachines **13**, 1102 (2022).

[64] R. J. Macfarlane, B. Lee, H. D. Hill, A. J. Senesi, S. Seifert, and C. A. Mirkin, "Assembly and organization processes in dna-directed colloidal crystallization," Proceedings of the National Academy of Sciences **106**, 10493–10498 (2009).

[65] R. V. Thaner, Y. Kim, T. I. N. G. Li, R. J. Macfarlane, S. T. Nguyen, M. Olvera de la Cruz, and C. A. Mirkin, "Entropy-driven crystallization behavior in dna-mediated nanoparticle assembly," Nano Letters **15**, 5545–5551 (2015).

[66] Y. Wang, Y. Wang, X. Zheng, É. Ducrot, J. S. Yodh, M. Weck, and D. J. Pine, "Crystallization of dna-coated colloids," Nature Communications **6**, 7253 (2015).

[67] J. D. Weeks, D. Chandler, and H. C. Andersen, "Role of repulsive forces in determining the equilibrium structure of simple liquids," The Journal of Chemical Physics **54**, 5237–5247 (1971).

[68] H. S. Ashbaugh and H. W. Hatch, "Natively unfolded protein stability as a coil-to-globule transition in charge/hydropathy space," Journal of the American Chemical Society **130**, 9536–9542 (2008).

[69] Y. Ding and J. Mittal, "Insights into dna-mediated interparticle interactions from a coarse-grained model," The Journal of Chemical Physics **141**, 184901 (2014).

[70] H. Seyforth, S. Chatterjee, T. E. Videbæk, M. Mondal, W. M. Jacobs, and W. B. Rogers, "The underappreciated role of nonspecific interactions in the crystallization of dna-coated

colloids," Soft Matter **21**, 2654–2663 (2025).

[71]M. S. Shell, "The relative entropy is fundamental to multiscale and inverse thermodynamic problems," The Journal of Chemical Physics **129**, 144108 (2008).

[72]M. S. Shell, "Coarse-graining with the relative entropy," in *Advances in Chemical Physics* (John Wiley & Sons, Inc, 2016) p. 395–441.

[73]A. N. Sreenivasan, C. L. Petix, Z. M. Sherman, and M. P. Howard, "relentless: Transparent, reproducible molecular dynamics simulations for optimization," The Journal of Chemical Physics **161**, 212502 (2024).

[74]C. L. Petix, M. Fakhraei, C. A. Kieslich, and M. P. Howard, "Surrogate modeling of the relative entropy for inverse design using smolyak sparse grids," Journal of Chemical Theory and Computation **20**, 1538–1546 (2024).

[75]J. A. Anderson, J. Glaser, and S. C. Glotzer, "Hoomd-blue: A python package for high-performance molecular dynamics and hard particle monte carlo simulations," Computational Materials Science **173**, 109363 (2020).

[76]W. B. Rogers and J. C. Crocker, "Direct measurements of dna-mediated colloidal interactions and their quantitative modeling," Proceedings of the National Academy of Sciences **108**, 15687–15692 (2011).

[77]W. Humphrey, A. Dalke, and K. Schulten, "Vmd: Visual molecular dynamics," Journal of Molecular Graphics **14**, 33–38 (1996).

[78]M. T. Casey, R. T. Scarlett, W. Benjamin Rogers, I. Jenkins, T. Sinno, and J. C. Crocker, "Driving diffusionless transformations in colloidal crystals using dna handshaking," Nature Communications **3**, 1209 (2012).

[79]J. Lowensohn, A. Hensley, M. Perlow-Zelman, and W. B. Rogers, "Self-assembly and crystallization of dna-coated colloids via linker-encoded interactions," Langmuir **36**, 7100–7108 (2020).

[80]H. Xiong, D. van der Lelie, and O. Gang, "Phase behavior of nanoparticles assembled by dna linkers," Physical Review Letters **102**, 015504 (2009).

[81]R. J. Macfarlane, M. R. Jones, A. J. Senesi, K. L. Young, B. Lee, J. Wu, and C. A. Mirkin, "Establishing the design rules for dna-mediated programmable colloidal crystallization," Angewandte Chemie International Edition **49**, 4589–4592 (2010).

[82]B. A. Lindquist, R. B. Jadrich, M. P. Howard, and T. M. Truskett, "The role of pressure in inverse design for assembly," The Journal of Chemical Physics **151**, 104104 (2019).

[83] A. Stukowski, "Structure identification methods for atomistic simulations of crystalline materials," Modelling and Simulation in Materials Science and Engineering **20**, 045021 (2012).

[84] P. M. Larsen, S. Schmidt, and J. Schiøtz, "Robust structural identification via polyhedral template matching," Modelling and Simulation in Materials Science and Engineering **24**, 055007 (2016).

[85] E. Maras, O. Trushin, A. Stukowski, T. Ala-Nissila, and H. Jónsson, "Global transition path search for dislocation formation in ge on si(001)," Computer Physics Communications **205**, 13–21 (2016).

[86] Y. Ma, J. C. Aulicino, and A. L. Ferguson, "Inverse design of self-assembling diamond photonic lattices from anisotropic colloidal clusters," The Journal of Physical Chemistry B **125**, 2398–2410 (2021).

[87] F. Romano and F. Sciortino, "Patterning symmetry in the rational design of colloidal crystals," Nature Communications **3**, 975 (2012).

[88] A. Hensley, W. M. Jacobs, and W. B. Rogers, "Self-assembly of photonic crystals by controlling the nucleation and growth of dna-coated colloids," Proceedings of the National Academy of Sciences **119**, e2114050118 (2022).

[89] A. Jain, J. R. Errington, and T. M. Truskett, "Dimensionality and design of isotropic interactions that stabilize honeycomb, square, simple cubic, and diamond lattices," Physical Review X **4**, 031049 (2014).

[90] N. A. Mahynski, R. Mao, E. Pretti, V. K. Shen, and J. Mittal, "Grand canonical inverse design of multicomponent colloidal crystals," Soft Matter **16**, 3187–3194 (2020).

[91] D. Chen, G. Zhang, and S. Torquato, "Inverse design of colloidal crystals via optimized patchy interactions," The Journal of Physical Chemistry B **122**, 8462–8468 (2018).

[92] E. M. King, C. X. Du, Q.-Z. Zhu, S. S. Schoenholz, and M. P. Brenner, "Programming patchy particles for materials assembly design," Proceedings of the National Academy of Sciences **121**, e2311891121 (2024).

[93] H. Liu, M. Matthies, J. Russo, L. Rovigatti, R. P. Narayanan, T. Diep, D. McKeen, O. Gang, N. Stephanopoulos, F. Sciortino, H. Yan, F. Romano, and P. Šulc, "Inverse design of a pyrochlore lattice of dna origami through model-driven experiments," Science **384**, 776–781 (2024).

[94] A. Trubiano and M. Holmes-Cerfon, "Thermodynamic stability versus kinetic accessibility: Pareto fronts for programmable self-assembly," Soft Matter **17**, 6797–6807 (2021).

[95] S. Chatterjee and W. M. Jacobs, "Multiobjective optimization for targeted self-assembly among competing polymorphs," Physical Review X **15**, 011075 (2024).

Data Availability Statement

The software used to perform the inverse design can be found at
https://github.com/mphowardlab/relentless. The parameters of the designed potentials
are available as supplementary information. The other data that supports the findings of
this study are available from the authors upon reasonable request.